Vibrational Lifetimes and Isotope Effects of Interstitial Oxygen in Silicon and Germanium

Kathryn Ellen Keister

Department of Physics, College of William and Mary

(Dated: May 7, 2004)

Abstract

The properties of a semiconductor crystal are significantly affected by the presence of impurities, whether they are necessary dopants or unwanted defect impurities. Light impurities give rise to local vibrational modes (LVMs) with frequencies higher than the lattice phonons of the pure crystal. The vibrational properties of these LVMs are important in characterizing the stability and diffusion of the defects that produced them. This thesis is specifically interested in determining the dynamics, that is the lifetimes, decay channels, and decay mechanisms of the LVMs of interstitial oxygen in silicon and germanium. The spectra of oxygen in Si and Ge show that the linewidth, which is inversely related to the lifetime, of the ^{17}O defect in Si is twice as broad as the ^{16}O and ^{18}O lines, and that the linewidths of Ge are ten times narrower than those in Si. These two features are not well understood, but direct lifetime measurements have corroborated the static spectral measurements, and a detailed examination of the theory of allowed decay channels for the excited state provides an explanation for these features.

Contents

List of Figures

List of Tables

I. INTRODUCTION

Semiconductors are an important class of materials distinguished from other materials by many physical properties, but most importantly, by their electric resistivity ρ or the resistance to electric current passing through the material. Materials with a resistivity larger than 10^{10}-10^{12} Ωcm are classified as insulators, while those with a resistivity less than 10^{-7}-10^{-9} Ωcm are classified as conductors. The materials somewhere in between are semiconductors. A semiconductor's resistivity is also highly temperature dependent, and in contrast to most conductors, decreases with higher temperature. Other characteristics of semiconductors include large impurity effects, both positive and negative charge carriers, and sensitivity to light. There are many solids that are classified as semiconductors. Group IV in the periodic table contains some of the most important, namely, silicon (Si) and germanium (Ge). Other common semiconductors are compounds such as GaAs, InSb, ZnSe, and PbTe.

In crystalline semiconductors, the ionized atoms form a periodic electric potential. The free electrons moving in this periodic potential have quantized energy levels. A semiconductor at 0K looks very much like an insulator; that is, certain energy bands are completely full, with the remaining bands completely empty. These bands that are empty at 0K are called the *conduction bands*. The gap between the highest full level and the lowest empty level is called the *fundamental gap*. In semiconductors, this gap is small enough that at higher temperatures, electrons can be excited into the conduction bands. The empty state, which such an electron leaves behind in an otherwise full level, is called a *hole* and can also carry current.

The properties of a semiconductor material are more strongly affected by the presence of impurities than are other types of materials. There are two types of electrically active impurities, *donor impurities*, which donate an electron to the conduction band, and *acceptor impurities*, which accept electrons from anywhere in the crystal. In silicon, elements from Group V of the periodic table, such as phosphorus (P), arsenic (As) and antimony (Sb) have one more valance electron than silicon, so they act as donor impurities and produce an n-type semiconductor, since the extra charge carriers are negative. Elements from Group III such as boron (B), aluminum (Al) and gallium (Ga) have one less valance electron, so they act as acceptors, forming a p-type

semiconductor with extra positive charge carriers (holes).

The functioning of semiconductor devices depends on very controlled introduction of impurities, called *doping*, of the semiconductor wafer. Dopants can produce conduction in the semiconductor at lower temperatures than would be required to thermally excite enough electrons to the conduction band [1]. However, unwanted impurities in a semiconductor crystal can contribute to the degradation of the device. The vibrational properties of defects in semiconductors, particularly the interaction dynamics and energy transfer mechanisms, are very important in determining the structure of these defects, and in characterizing their stability, migration and reactions.

The structure of the defects can be understood by frequency-domain measurements, such as an Fourier transform infrared (FTIR) spectrum. Very high resolution spectra and very accurate measurements have been taken of the linewidth of the absorption spikes in the infrared (IR) spectrum that correspond to the defects. From these static measurements, we note several interesting points that can be further illuminated by high resolution time domain measurements of the lifetime (the lifetime being related inversely to the linewidth of the absorption peak), as well as by some theoretical discussion.

While the structure and static properties of many defects have been studied, their dynamics are often not well understood. The defects produce localized vibrational states, which have excited states. The processes we are trying to illuminate include how the excited states couple to the phonon bath of the solid, the relaxation path and the lifetimes of the excited states. Direct time domain measurements of the lifetimes of the excited vibrational states are now possible because of recent advances in tunable, ultrafast IR light sources, including optical parametric amplifiers (OPAs) and free-electron lasers (FELs). Such studies are useful in understanding the energy transfer pathways at defects and impurities in semiconductors.

In this thesis, the system under study is interstitial, meaning along the bond axis, oxygen in silicon and germanium, where the oxygen is bonded to two Si or Ge atoms. The oxygen defects have three natural isotopes: ^{16}O, ^{17}O, and ^{18}O. From the frequency-domain measurements, we note that the linewidth of the ^{17}O line in Si is twice that of the ^{16}O and ^{18}O lines. Also, the linewidths of all of the isotopes in Ge

are almost ten times narrower than those in Si. A possible explanation for both of these observations is found in the relaxation and decay mechanism and the coupling of the LVM to the phonon bath.

II. THEORETICAL BACKGROUND

A. Crystal Structure

The study of crystalline solids forms a large portion of condensed matter physics. Crystals as they are found in nature or grown in a lab are finite regular arrangements of atoms. These finite arrangements are never perfect in practice, but can be approximated by perfect infinite geometrical arrays of points called *lattices*. A lattice is defined as "an infinite set of points in space so arranged that every point has identical surroundings." [2] It turns out that there are only 14 unique ways of arranging points so that they have identical surroundings. These arrays are called the *Bravais lattice arrays*. This does not mean that there are only 14 crystals structures, since many different groups of atoms can be associated with a lattice point. The standard volume that is used to identify and describe a particular structure is called the *crystallographic unit cell*. Silicon (Si) and Germanium (Ge) are derived from the face-centered cubic Bravais lattice. This is also called the *diamond structure*, since it is the arrangement of the carbon atoms in diamond crystals [2]. The unit cell of the diamond structure is shown in Figure 1.

The periodicity of the crystal structure leads to a periodic division of the wave vector or momentum space into what are called *Brillouin zones*. These are defined by the Bragg planes that bisect a set of vectors from the origin to the lattice points that define the unit cell. The first Brillouin zone for the diamond structure is shown in Figure 2. The Cartesian directions are indicated, but the more useful reference points are the high symmetry points marked. The Γ point is the point of highest symmetry, here located at the center of the unit cell.

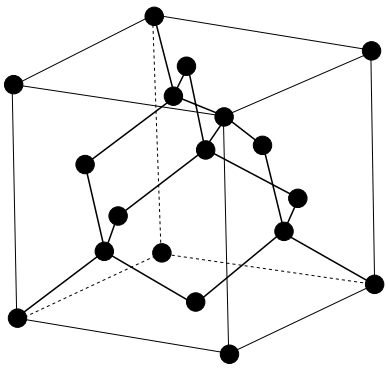

FIG. 1: Diamond crystal structure unit cell

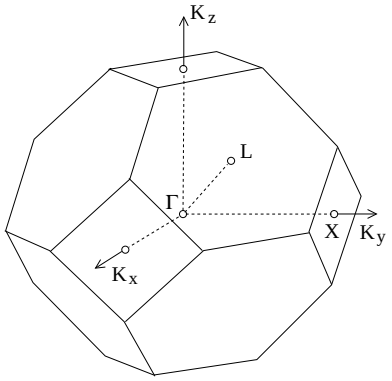

FIG. 2: Brillouin zone of the diamond structure with high symmetry points indicated

B. Lattice vibrations and phonons

The atoms in a pure crystal solid, such as a semiconductor, oscillate collectively about their equilibrium positions, resulting in quantized vibrational modes, called *phonons*. A pure crystal has a well defined set of characteristic frequencies of vibration, called the phonon bath. These phonons involve the motion of many atoms, so they are extended in real space. They are also extended in frequency space, as the phonon bath covers a band of frequencies. While a full calculation of the energy and momentum distribution of the phonons allowed in a particular crystal structure is beyond the scope of this thesis, a number of approximations of increasing complexity give good first order results, and are included in Appendix A.

This relation between the allowed vibrational frequencies ω and their wave vectors, $\vec{k}$ is called the phonon dispersion curve. Full *ab initio* calculations are available in the literature [3–5]. Specific features that prove relevant are the splitting of the curve into optical and acoustic branches, and again into transverse and longitudinal branches. Phonons are classified into these four categories (listed in order of decreasing frequency and energy): transverse optical (TO), longitudinal optical (LO), longitudinal acoustic (LA), and transverse acoustic (TA).

The dispersion curves in Figure 3 are for Si and Ge. The graphs on the far right side are the density of states plots, which are obtained by integrating over the dispersion curves, giving the distribution of the density of phonon modes as a function

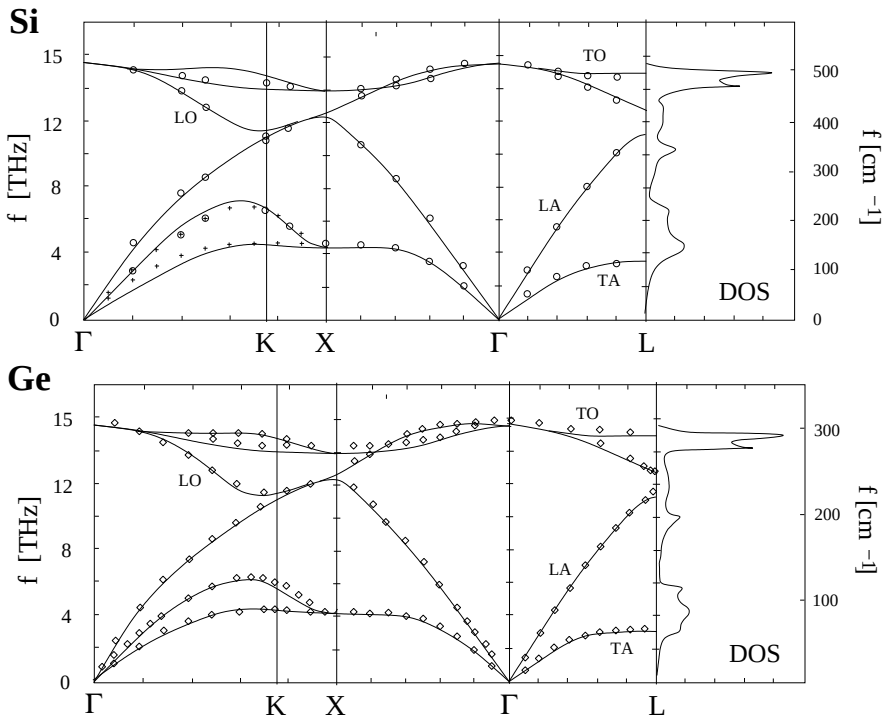

FIG. 3: Phonon dispersion curve and density of states for silicon (top) and germanium (bottom). Si figure courtesy of Wei [4], Ge figure courtesy of Giannozzi et al. [3].

of frequency, here in THz, or as a function of wavenumber, in cm^{-1}. The two elements have identical crystal structure, so their dispersion and density of states curves are very similar, with Ge having lower frequencies because its mass is higher than Si.

A phonon can exchange energy with radiation (photons) or with particles, and these interactions must conserve energy (related to frequency) and momentum (related to the wavevector). Phonon-dispersion relations can therefore be determined experimentally by scattering particles or radiation (photons) off the phonons in a crystal. The typical energies of phonons are 0.01 eV, and this small energy limits the types of particles that can be used to probe the crystal solid. Electromagnetic radiation has too high an energy (keV), as do electrons (about 16 eV). Solids also very readily absorb electrons, which prevents an effective scattering experiment. Neutrons, on the other hand, have an energy about the same as that of phonons, and their lack of charge and high penetration makes them ideal for study of phonon dispersion. Inelastic neutron scattering is used extensively to measure phonon-dispersion curves. The markers along the curves in Figure 3 are experimental data points.

C. Local vibrational modes

Introduction of an impurity destroys the crystal symmetry; in addition to altering the electronic properties of the sample, it also alters the vibrational properties and new vibrational modes may appear. Impurities that are lighter than the host lattice atom will give rise to higher frequency vibrational modes that are above the phonon band of the pure solid. These modes are called *local vibrational modes* (LVMs), as they are localized in both the real space domain and the frequency domain, while the lattice phonons are not. Because of this localization, they show up as sharp lines in the infrared (IR) absorption spectrum of the crystal sample [6].

The coupling between the LVMs and the phonon bath of the host crystal describes the flow of energy into and out of impurity and defect complexes. This energy flow can be significant because the electronic excitation that is deposited at the defects is then available to promote defect migration and reactions, which has an important influence on the degradation of semiconductor devices. The energy relaxation of these LVMs involves redistributing the energy of the excited vibrational state to low-frequency vibrational modes that are coupled inelastically to the local excited state. Typical energy relaxation times are hundreds of femtoseconds to hundreds of picoseconds.

While high-resolution absorption spectra are available, the lifetime generally cannot be accurately derived from the linewidth because of the extremely short time scales that characterize the elastic transitions leading to dephasing of the vibrational transition and linewidth broadening. Furthermore, inhomogeneous effects may contribute significantly to the measured absorption linewidth.

The function describing the LVM absorption peaks is generally given by a convolution of the homogeneous linewidth with a function describing the inhomogeneous broadening. Inhomogeneous broadening can result from the strain fields induced by the lattice defects in the sample. These strain fields can be reduced–and therefore the inhomogeneous contribution to the linewidth also reduced–by lowering the defect concentration in the sample. The homogeneous linewidth is then

$$\Gamma_H = \frac{1}{2\pi c T_1} + \frac{1}{\pi c T_2^*}, \tag{II.1}$$

where T_1 is the lifetime of population relaxation, and determines the natural linewidth of the mode, and T_2^* is the time of phase relaxation (pure dephasing). At low temper-

atures, elastic scattering of the local mode with phonons is reduced, and the first term dominates, and the natural linewidth, Γ_0, can then be used to give a good estimate of the vibrational lifetime by the following equation [7]:

$$T_1 = \frac{1}{2\pi c \Gamma_0}. \tag{II.2}$$

The particular defect that produces the LVM we study is interstitial oxygen in semiconductors. Oxygen in silicon was one of the first impurities studied using vibrational spectroscopy [8]. In an early study, Kaiser et al. [9] measured the IR absorption of silicon, and identified a 9μm (1106 cm^{-1}) absorption band with oxygen content in the samples. They suggested a model of an interstitial type defect, with the oxygen atom bonded to its two neighboring Si atoms.

There are three types of vibrational motion that this defect exhibits. Shown in Figure 4 are the vibrational modes of the interstitial oxygen defects in both Si and Ge. The silicon modes are labeled with the representations of the D_{3d} point group to

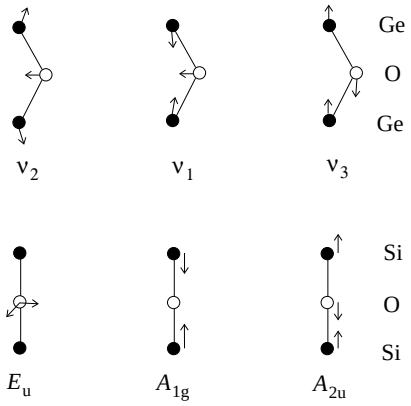

FIG. 4: Vibrational modes of interstitial oxygen in germanium (top) and silicon (bottom). Figure courtesy of Artacho [10]

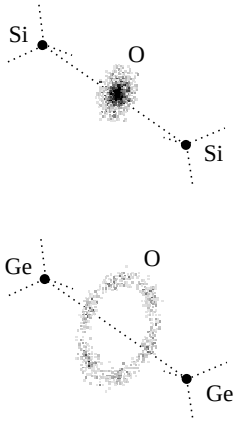

FIG. 5: Delocalization of oxygen in Si and Ge. Figure courtesy of Artacho [10]

which they belong (discussed further in Appendix B). The modes are called, left to right, the bending mode, the symmetric stretch mode, and the anti-symmetric stretch mode. The anti-symmetric, also called asymmetric, stretch mode was identified with the 1136cm^{-1} absorption band by Hrostowski et al. [11]. The bending mode has two orthogonal states, but because the bond angle of the Ge compound is smaller than that of Si (172° in Si, and 140° in Ge), the bending motion in Ge is more of a circular

motion around the bond axis, and the O atom is unlikely to move toward the bond axis (see Figure 5) [10].

Recently, McCluskey et al. have studied the resonant interactions between the asymmetric stretch local mode in ^{18}O and a spatially extended mode using hydrostatic pressure. The authors state that this transition from a localized to an extended mode is the first step toward the decay into lattice phonons [12].

D. Multiphonon decay

The energy of the asymmetric stretch mode in Si is 1136cm^{-1}, but silicon's phonon bath only spans an energy range up to about 522cm^{-1}. Therefore, since the energy of the excited state exceeds the energy of a single phonon, more than one phonon will be created in the decay process. This is called *multiphonon relaxation*, and has been derived by Nitzan et al. [13]. The Hamiltonian of the system can be written

$$H = H_{LVM} + H_{BATH} + H_{INT}, \tag{II.3}$$

where H_{LVM} describes the ground and excited states of the LVM, H_{BATH} is the Hamiltonian of the phonon bath in the crystal, and H_{INT} describes the interaction between the LVM and the phonon bath. The simplest quantum mechanical model for an LVM is the harmonic oscillator. The coupling of the LVM to the phonon bath requires the anharmonic corrections described by H_{INT}. Expanding each of the terms in Eq. II.3, we find

$$H_{LVM} = \hbar\omega a^{\dagger} a, \tag{II.4}$$

which is the Hamiltonian for a simple harmonic oscillator,

$$H_{BATH} = \sum_{\{\nu\}} \sum_{i=1}^{N_\nu} \hbar\omega_i^{\{\nu\}} b_{i,\{\nu\}}^{\dagger} b_{i,\{\nu\}}, \tag{II.5}$$

where each decay channel $\{\nu\}$ is characterized by the set $\{\omega_1^{\{\nu\}}, \omega_2^{\{\nu\}}, ..., \omega_{N_\nu}^{\{\nu\}}\}$ of accepting mode frequencies. In addition, energy must be conserved in the decay process, that is, $\hbar\omega = \sum_{j=1}^{N_\nu} \hbar\omega_j^{(\nu)}$. The interaction between the LVM and the phonon bath produces an anharmonic perturbation in the harmonic H_{LVM}, which can be treated

by first-order time-dependent perturbation theory. The coupling Hamiltonian is

$$H_{INT} = \sum_{\{\nu\}} \hbar(G_{\{\nu\}} B_{\{\nu\}} a^\dagger + G^*_{\{\nu\}} B^\dagger_{\{\nu\}} a) \tag{II.6}$$

where $G_{\{\nu\}}$ is the coupling strength and $B_{\{\nu\}}$ and $B^\dagger_{\{\nu\}}$ are the products of the creation and annihilation operators for all of the frequencies of a decay channel, given by $B_{\{\nu\}} = \prod_{i=0}^{N_{\{\nu\}}} b_{i,\{\nu\}}$ and $B^\dagger_{\{\nu\}} = \prod_{i=0}^{N_{\{\nu\}}} b^\dagger_{i,\{\nu\}}$.

The contribution to the decay rate due to H_{INT} is given by the standard first-order perturbation theory result, and the total decay rate is given as the sum of the rates of all the decay channels,

$$\frac{1}{T_1} = \Gamma = 2\pi \sum_{\{\nu\}} |G_{\{\nu\}}|^2 n_{\{\nu\}} \rho_{\{\nu\}} \tag{II.7}$$

The function $n_{\{\nu\}}$ is the thermal population of the accepting modes, given by the Bose-Einstein distribution,

$$n_{\{\nu\}} = \frac{\exp(\hbar\omega/k_B T) - 1}{\prod_{j=1}^{N_\nu} [\exp(\hbar\omega_j^{(\nu)}/k_B T) - 1]} \tag{II.8}$$

In the low temperature limit, $n_{\{\nu\}} \cong 1$, and does not affect the decay rate. So the decay rate depends on $\rho_{\{\nu\}}$, the spectral density of accepting states [13, 14].

III. EXPERIMENTAL TECHNIQUES

A. Fourier-transform infrared spectroscopy

Fourier-transform infrared (FTIR) spectroscopy is used widely in many areas of physics, chemistry, and biology as a characterization technique. FTIR spectrometers produce a low noise frequency-domain spectrum over a broad spectral range in a relatively short amount of time. The main component of an FTIR spectrometer is a Michaelson interferometer (see Figure 6).

The broadband source emits radiation at all IR wavelengths in a collimated beam, which travels through a beam splitter. One beam is reflected off a fixed mirror and the other off a movable mirror. The two beams recombine, travel through the sample and are collected by a detector. The detector produces an *interferogram*, which is

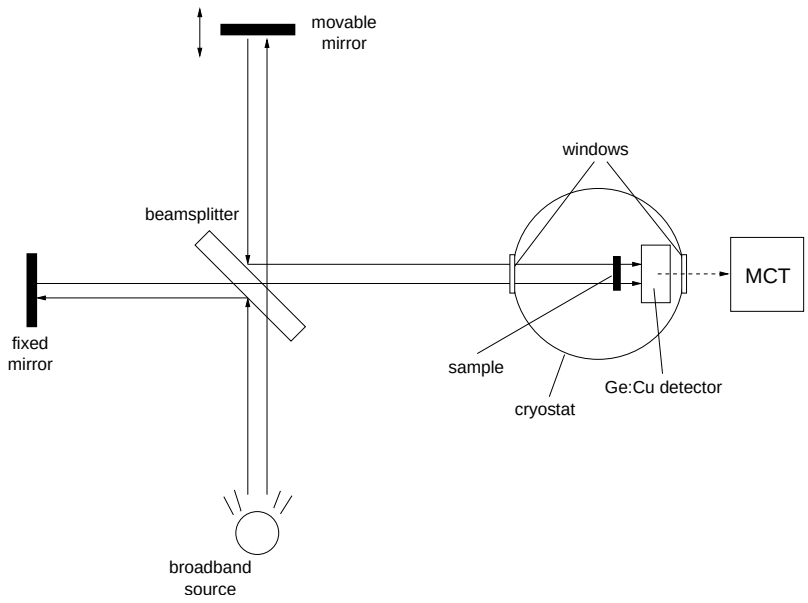

FIG. 6: Schematic diagram of an FTIR spectrometer. Figure courtesy of McCluskey [6]

a plot of intensity of the interfered beam versus path difference between the fixed and movable mirrors. To maximize the signal-to-noise ratio, up to several thousand interferograms are taken and the results averaged [6].

For a single frequency of light of wavenumber k, the intensity of the interferogram I_k is given by the traditional two-beam interference relation

$$I_k(x) = J(k)\left[1 + \cos(kx)\right], \tag{III.1}$$

where $J(k)$ is the incident intensity of the broadband source as a function of frequency, and x is the path difference between the two beams. Since the source contains more than one frequency, the interferogram shows a superposition of intensities

$$I(x) = \int_0^\infty J(k)\left[1 + \cos(kx)\right] dk. \tag{III.2}$$

This can be written as the sum of the mean value of the interferogram plus the intensity as a function of x:

$$\int_0^\infty J(k)dk + \int_0^\infty J(k)\cos(kx)dk = \overline{I(x)} + \int_0^\infty J(k)\cos(kx)dk. \tag{III.3}$$

The spectral distribution $J(k)$ can be recovered by subtracting the mean value $\overline{I(x)}$ and taking the inverse Fourier transform:

$$J(k) = \int_0^\infty I(x)\cos(kx)dx. \tag{III.4}$$

The result is a frequency-domain plot of the intensity of the interferogram as a function of the frequency, low intensity indicating high absorption by the sample and vice versa [15].

FTIR spectra for the interstitial oxygen defect are shown in Section IV A, Figures 9 and 10.

B. Optical parametric amplification

For time-domain spectroscopic measurements, it is essential to have high-power, ultrafast laser sources that continuously span the spectrum of interest. In the past, dye and solid-state lasers have been the major sources of picosecond pulses, but they have very limited tuning range. Nonlinear optical effects have long been used for frequency conversion, but recent technical advances in the quality of the nonlinear crystals and in the pump lasers have led to the development and commercial availability of highly tunable laser systems called *optical parametric devices*. The basic spontaneous optical parametric process is a quantum-field effect that results in one high frequency photon annihilating and producing two lower frequency photons. In an optical parametric device, the high frequency photon is the pump, ω_p, and the low frequency photons are the signal, which is somewhat arbitrarily chosen as the higher frequency of the two, ω_s and the idler, ω_i. Energy conservation requires that $\omega_p = \omega_s + \omega_i$. The functioning of these devices depends on the polarization properties of the crystal material. The polarization $\vec{P}$ is defined as

$$\vec{P}(\vec{r},t) = \varepsilon_0(\chi^{(1)}\vec{E} + \chi^{(2)}\vec{E}^2 + \chi^{(3)}\vec{E}^3 + ..., \qquad \text{(III.5)}$$

where the $\chi^{(i)}$ are the electric susceptibility of the crystal. In linear materials, and at low electric field, only the first term is significant. In crystals with a high second-order (nonlinear) optical polarization, the second-order polarization becomes significant. Optical parametric amplification (OPA) is a three-wave mixing process, and the pump

beam, the signal, and the idler are coupled by the second-order polarization tensor:

$$\begin{aligned}\vec{P}^{(2)}(\vec{r},t) &= \varepsilon_0 \overset{\leftrightarrow}{\chi}^{(2)} (\omega_s = \omega_p - \omega_i) : \vec{E}_p \vec{E}_i^* \exp[i(\vec{k}_p - \vec{k}_i)\cdot\vec{r} - i\omega_s t] \\ &+ \varepsilon_0 \overset{\leftrightarrow}{\chi}^{(2)} (\omega_i = \omega_p - \omega_s) : \vec{E}_p \vec{E}_s^* \exp[i(\vec{k}_p - \vec{k}_s)\cdot\vec{r} - i\omega_i t] \\ &+ \varepsilon_0 \overset{\leftrightarrow}{\chi}^{(2)} (\omega_p = \omega_s + \omega_i) : \vec{E}_s \vec{E}_i \exp[i(\vec{k}_s + \vec{k}_i)\cdot\vec{r} - i\omega_p t] \\ &+ \text{other nonlinear terms.}\end{aligned} \tag{III.6}$$

Clearly, the coupling strength is determined by the strength of the nonlinear response $\overset{\leftrightarrow}{\chi}^{(2)}$. The solution to Maxwell's wave equation

$$\vec{\nabla}^2 \vec{E}(\vec{r},t) - \mu_0 \varepsilon_0 \frac{\partial^2}{\partial t^2} \vec{E}(\vec{r},t) = \mu_0 \frac{\partial^2}{\partial t^2} \vec{P}^{(2)}(\vec{r},t) \tag{III.7}$$

contains three components, the pump, the signal, and the idler

$$\vec{E}(\vec{r},t) = \frac{1}{2}\left[\vec{E}_p(\vec{r}) e^{i\vec{k}_p\cdot\vec{r} - i\omega_p t} + \vec{E}_s(\vec{r}) e^{i\vec{k}_s\cdot\vec{r} - i\omega_s t} + \vec{E}_i(\vec{r}) e^{i\vec{k}_i\cdot\vec{r} - i\omega_i t} + \text{complex conjugates}\right]. \tag{III.8}$$

If the pump depletion is assumed to be negligible, $\vec{E}_p$ can be regarded as constant, and $I_p(z) = I_p(0)$. In an OPA system, there is a small input-signal intensity $I_s(0)$, generally from a white light source. As the two beams propagate in the crystal, the signal beam is amplified by coupling with the pump beam. The output intensities for beams traveling in the z-direction are given by

$$\begin{aligned} I_s(z) &= I_s(0)\cosh^2(gz) \\ I_i(z) &= I_s(0)\frac{\omega_i}{\omega_s}\sinh^2(gz) \\ I_p(z) &= I_p(0). \end{aligned} \tag{III.9}$$

The coefficient g is the gain

$$g = \sqrt{g_0^2 - \frac{\Delta\vec{k}^2}{4}}, \quad g_0 \propto \chi^{(2)}_{eff} I_p^{1/2} \tag{III.10}$$

where g_0 is the steady-state small signal gain. To maximize the gain, then, we want a high pump intensity I_p, which requires a crystal with a high damage threshold as well as a high $\chi^{(2)}$. The second term describes the phase matching condition, $\Delta\vec{k} = \vec{k}_p - \vec{k}_s - \vec{k}_i$, for which the maximum gain occurs at $\Delta\vec{k} = 0$. The phase matching condition can be expanded to $\Delta k = \frac{\omega_p}{c} n_p - \frac{\omega_s}{c} n_s - \frac{\omega_i}{c} n_i$, and we know from

energy conservation that $\omega_p - \omega_s - \omega_i = 0$, and c is a constant, so $\Delta k = 0$ if $n_p = n_s = n_i$. In general, this will not be true, since most crystals are dispersive and have an index of refraction that depends on the frequency. The solution is to use *birefringent* crystals, whose index of refraction is different for different polarizations of incident light. Light polarized parallel to the optic axis of the crystal has a different index of refraction, and one that is dependent on the angle between the incident ray and the optic axis. This ray is called the *extraordinary ray*. Light polarized perpendicular to the optic axis behaves normally, and is called the *ordinary ray*. Birefringence can be used to compensate for the dispersion of the medium by polarizing the pump beam perpendicular to the signal and idler beams. The angle of the crystal determines the frequencies of the signal and idler, because the phase matching condition will be met only for a specific frequency pair. The frequency can be tuned, therefore, by changing the angle, or, in some cases, the temperature of the crystal, which would change its index of refraction. Figure 7 shows the OPA process, with three beams going into the nonlinear crystal, the signal and idler polarized perpendicular to the optic axis (c-axis) and the pump polarized parallel to it. The tuning angle is the angle between the propagation vector $\vec{k}$ of the pump beam and the optic axis.

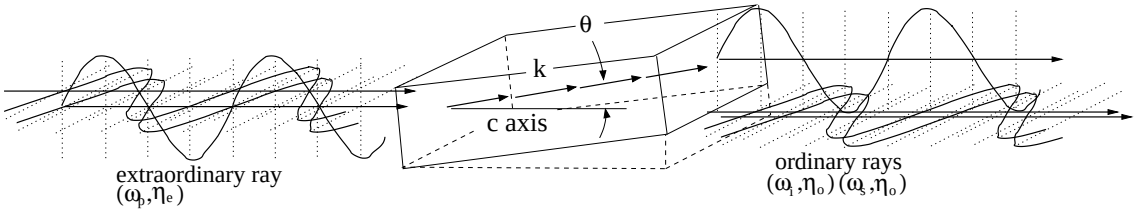

FIG. 7: The OPA process

For a crystal to be suitable for an OPA laser system, it must have sufficiently large nonlinearity and high damage threshold, and must also have low absorption at the pump and signal frequencies. Lasers constructed using an OPA system have no cavity, so the single pass gain must be very high, and they therefore must be pumped by a high power laser. Common pump lasers include mode-locked solid-state lasers such as Ti-sapphire and Nd:YAG, and their harmonics [16, 17].

The laser system used for the measurements in Section IV B is a traveling-wave optical parametric amplifier of superflourescence (TOPAS) pumped with the funda-

mental of a Ti-sapphire laser at 800nm. The seed signal beam that is amplified is generated using superflourescence by tightly focusing part of the pump beam on the crystal. The signal and idler of the OPA nonlinear crystal are output to another nonlinear crystal that does a difference frequency generation (DFG) using a similar process as the OPA to produce a beam at $\omega_{output} = \omega_s - \omega_i$. The system runs at a repetition rate of 1kHz with a pulse duration of 2ps, spectral width of 15-20cm^{-1}, and a pulse energy of 18μJ at 1136cm^{-1} (8.8μm) and 1109cm^{-1} (9μm), and 9μJ at 861cm^{-1} (11.6μm).

C. Pump-probe lifetime measurements

The lifetime of the excited state can be approximated from the linewidth of the FTIR spectrum, but can be more accurately determined by direct measurement using the pump-probe transient bleaching technique. This technique uses ultrashort pulses from a tunable infrared laser, either an optical parametric amplifier (OPA) or a free-electron laser (FEL). Free-electron lasers have a higher repetition rate, on the order

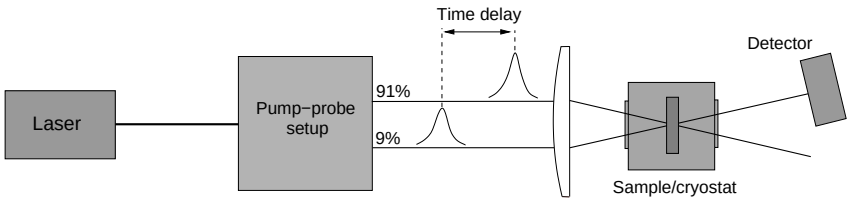

FIG. 8: Schematic diagram of the pump-probe setup

of MHz, as compared to OPA repetition rates in the kHz range, and they are also more stable. The measurements included in Section IV B were done with an OPA laser.

The schematic for a typical pump-probe experiment is shown in Figure 8. It is also a form of a Michaelson interferometer. The laser beam, tuned to the frequency of the vibrational mode, is split into two parts: the pump beam, which carries 91% of the power, and the probe beam, which carries the remaining 9%. The two beams are overlapped on the sample. The pump beam excites a fraction of the Si-O-Si or Ge-O-Ge bonds to their excited state, up to a maximum of 50%, which causes an increase in the transmission coefficient of the sample, since there are fewer LVMs in

the ground state to absorb the photons. The transmission coefficient then decreases over time as the excited modes decay back to the ground state and are available to absorb the incident photons of the probe beam. The decaying transmission is measured by varying the time delay between the pump and probe pulses, and the lifetime of the excited mode can be determined. The intensity of the probe beam is measured using a liquid nitrogen cooled HgCaTe detector [7].

IV. RESULTS

A. FTIR absorption spectra

There are three natural isotopes of oxygen, ^{16}O,^{17}O, and ^{18}O. Because the vibrational frequency depends on the mass of the atoms involved, defects including different isotopes have slightly different frequencies. In silicon, the absorption line of the ^{17}O defect is twice as broad as the ^{16}O and ^{18}O lines. Current theories offer no good explanation for this. The broadening of the ^{17}O line is independent of the concentration of the defect. Pajot et al. proposed that the broadening was due to spin differences between the isotopes [18], but we do not see it in the Ge spectrum or in the other vibrational modes in Si, so the broadening is not simply due to the ^{17}O isotope itself. There are also isotopes of Si, but the effects are much smaller, producing only small sidebands in the spectra. In Figure 9, the O isotopes are labeled and the linewidths are listed.

Germanium has five natural isotopes (^{70}Ge, ^{72}Ge, ^{73}Ge, ^{74}Ge, ^{76}Ge), so the absorption spectra is much more complicated (see Figure 10), and the isotope of the Ge atoms has a significant effect. The linewidths of the oxygen defects in Ge are much narrower than those in Si, on the order of ten times narrower (0.04 cm^{-1} in Ge vs. 0.55 cm^{-1} in Si). This large difference in linewidths has also not been explained. In Figure 10, a typical linewidth is indicated and the peaks are labeled with the average atomic mass of the two Ge atoms in the defect pseudo-molecule.

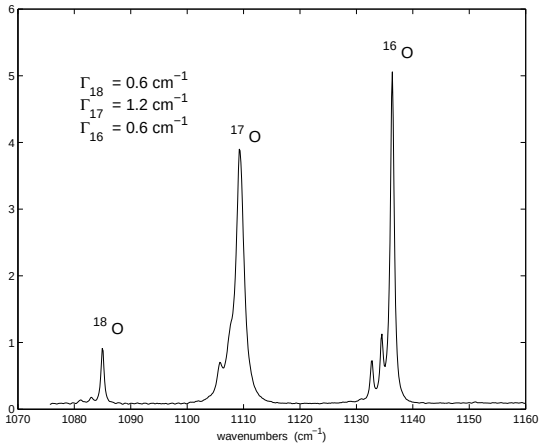

FIG. 9: Silicon FTIR spectrum[18]

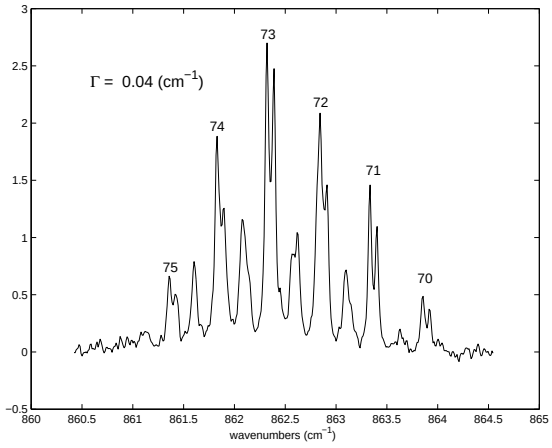

FIG. 10: Germanium FTIR spectrum[19]

B. Lifetime measurements

The direct measurements of the lifetimes were done at Jefferson Lab's FEL facility using the TOPAS laser system described above in Section III B. The silicon sample used for the measurement was enriched with oxygen isotopes by diffusion. The concentrations of ^{16}O, ^{17}O, and ^{18}O are 20, 25, and 2.4 $\times$ 10^{16} cm^{-3} respectively. The germanium sample contains all five germanium isotopes at their natural relative concentrations and ^{16}O at a concentration of 4.9 $\times$ 10^{16} cm^{-3}. The samples were mounted in an evacuated cryostat to allow for low temperature measurements.

Figure 11 shows a semi-log plot of the transient bleaching signal S_b vs. time delay for ^{16}O and ^{17}O in Si at 10K. The concentration of ^{18}O was too low for a measurement to be made. Both plots show a good fit to single exponentials with time constants that give decay times of T_1=11.5 $\pm$ 1ps for ^{16}O and T_1=4.5 $\pm$ 0.4ps for ^{17}O. The solid line in Figure 11(a) is measured at a frequency between the two modes, and does not show the decay, which indicates that the TOPAS spectrum is narrow enough to resolve the two isotopes. Figure 12 shows a similar plot of the ^{16}O in germanium, with a decay time of T_1=125 $\pm$ 10ps. The laser spectrum is not narrow enough to resolve the germanium isotopes, so this represents an average over all possible pseudo-molecule combinations.

Using Eq. II.2, the linewidth of the absorption spectra can be calculated from the lifetimes. This calculation gives a result of 1.12cm^{-1} for ^{17}O in Si, 0.44cm^{-1} for ^{16}O

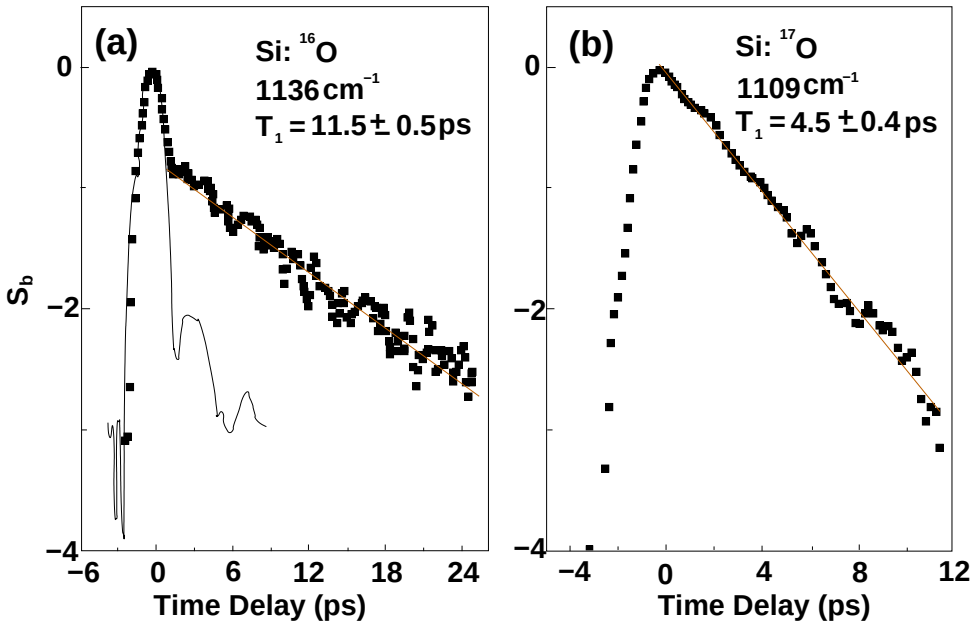

FIG. 11: Transient bleaching signal (S_b) vs. time for ^{16}O and ^{17}O in Si

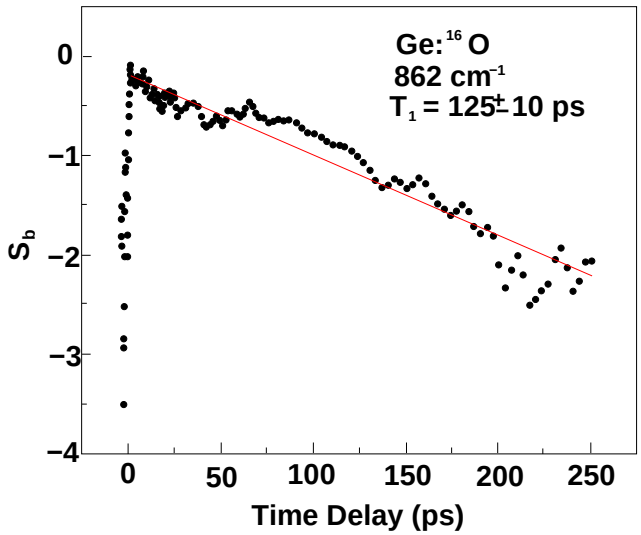

FIG. 12: Transient bleaching signal (S_b) vs. time for ^{16}O in Ge

in Si, and 0.04cm^{-1} for ^{16}O in Ge. These correspond well to the frequency-domain measurements, indicating that at low temperature, the absorption lines of interstitial oxygen are homogeneously broadened and dominated by the natural linewidths. A summary of the results and comparison to frequency domain measurements (discussed in Section IV A) is shown in Table I.

sample	measured lifetime	linewidth from lifetime	linewidth from FTIR
^{17}O in Si	4.5±0.4ps	1.12cm^{-1}	1.2cm^{-1}
^{16}O in Si	11.5±0.5ps	0.44cm^{-1}	0.6cm^{-1}
^{16}O in Ge	125±10ps	0.042cm^{-1}	0.04cm^{-1}

TABLE I: Summary of measured lifetimes and comparison to frequency domain measurements of linewidth

V. DISCUSSION

A. Multiphonon decay channels

In Section IV A above, I noted that the broadening of the ^{17}O line could not be a function simply of the isotope, and because it does not appear in the other vibrational modes (symmetric stretch and bending), this effect cannot be a broadening of the ground state. Therefore, the broadening of the absorption line must be related to the excited vibrational state and the decay mechanism of that state. The decay mechanism was derived in Section II D, and the relevant quantity in the low temperature limit was found to be the spectral density of accepting states.

The multiphonon spectral density of states can be expressed in terms of a convolution of the single spectral densities of states (which are derived from the phonon dispersion curve as described in Section II B and Appendix A). A Convolution is an integral which expresses the overlap of one function g as it is shifted over another function f. A convolution is calculated as

$$f * g = f \otimes g = \int_{-\infty}^{\infty} f(\tau)g(t-\tau)d\tau = \int_{-\infty}^{\infty} g(\tau)f(t-\tau)d\tau \qquad \text{(V.1)}$$

The phonon band of Si only goes up to 522 cm^{-1}, and the anti-symmetric stretch mode of the oxygen defect has a frequency ranging from 1085-1135 cm^{-1}, depending on the oxygen isotope. This mode, therefore, falls in the three-phonon density of states in Si. In Ge also, the anti-symmetric stretch mode is in the three-phonon density of states. Figures 13 and 14 show the three-phonon density of states of silicon and germanium, and the three oxygen isotope lines, left to right on each graph, ^{18}O, ^{17}O, and ^{16}O

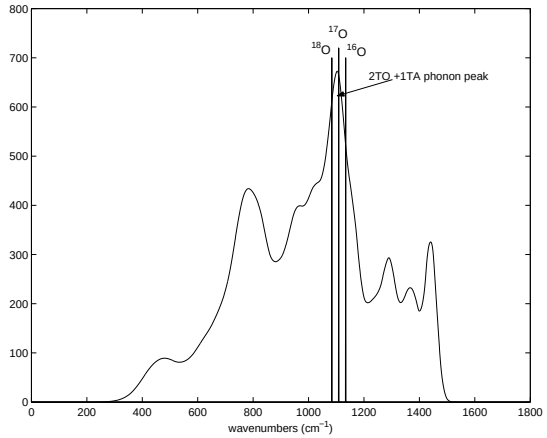

FIG. 13: Silicon three-phonon density of states

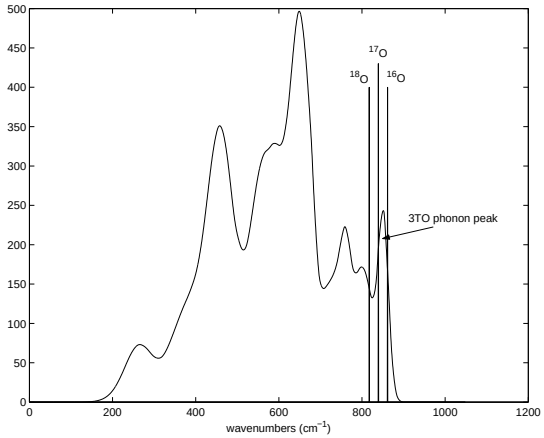

FIG. 14: Germanium three-phonon density of states

In the Si figure, the ^{17}O line is found to fall on a peak with the highest phonon density, while the ^{16}O and ^{18}O lines fall off to the side slightly. The peak is quite steep, so this results in a significant difference in the phonon density of states at the frequencies of vibration for the different oxygen isotopes. This difference in phonon densities explains the wider linewidth of the ^{17}O in the FTIR spectrum. The ^{17}O mode has a higher density of phonons to couple to, resulting in a shorter lifetime and a wider linewidth.

A comparison of the Si and Ge figure indicates that the average density at the frequencies of the oxygen defects in Ge is about a third of that in Si. A lower density of accepting phonon modes would increase the lifetime, and reduce the linewidth, but the difference in linewidth is almost ten times, which is not adequately explained by a factor of three in density. One remaining distinction is the phonon combination of the accepting modes. As explained in Section II B and Appendix A, there are four branches of phonons. The oxygen lines in silicon fall on the peak corresponding to 2TO phonons and 1TA phonon, while in germanium, it is the 3TO phonon peak. The energy and momentum are already constrained to be conserved, so the only remaining conservation rule we can apply is symmetry, and since the phonon combinations are different, they will have different symmetries.

B. Activity of accepting modes

A local vibrational mode (LVM), such as those indicated in Figure 4, can be probed by one of two main spectroscopic methods, Raman scattering and infrared (IR) spectroscopy. A mode's *activity* describes which of these processes it responds to. The experiment discussed in Section IV B is an example of IR spectroscopy. The activity of a mode can be determined using symmetry selection rules based on the group theory formalism discussed in Appendix B, since the transition from ground to excited state must conserve symmetry. Both types of activity, and how to determine a mode's activity, are described further in Appendix C.

The other interaction that requires symmetry selection rules is the decay of the excited vibrational mode into the phonon bath of the crystal. This decay transition must also conserve symmetry. The anti-symmetric stretch mode falls in the three-phonon density of states, and the three-phonon combination that the excited state decays into is called the decay channel. In order to determine the allowed decay channels, it is necessary to calculate the symmetry of the three-phonon combinations.

The symmetry and selection rules of two- and three-phonon combinations in diamond-type crystals are discussed and calculated by Birman [20, 21]. For transitions where all of the elements are at the same symmetry point and are described by the same point group, the total symmetry can be calculated as the direct product of the elements. For IR and Raman activation (discussed further in Appendix C) the product is

$$\Gamma[\psi(\nu')] \otimes \Gamma[\hat{\wp}] \otimes \Gamma[\psi(\nu)], \tag{V.2}$$

where $\hat{\wp}$ is the operator describing the IR or Raman transition from $\psi(\nu)$ to $\psi(\nu')$. These products are generally reducible to a direct sum of irreducible representations of the point group, and the mode is active if the direct sum contains the totally symmetric irreducible representation.

Calculating the symmetry of three-phonon combinations is complicated because the phonons can occur at different symmetry points, and thus have different symmetry point groups. For example, the interstitial oxygen defect occurs at the L-point, which has D_{3d} symmetry, but one of the allowed phonon decay channels is TO(L) + TA(L) + TO(X). Two of the phonons are at the L-point, but one is at the X-point, and therefore

has different symmetry. In general, the symmetry of a three-phonon combination mode consisting of phonons with wavevectors $\vec{k}_1$, $\vec{k}_2$, and $\vec{k}_3$ is the direct product of their irreducible representations:

$$^\star\vec{k}_1 \otimes {}^\star\vec{k}_2 \otimes {}^\star\vec{k}_3 \tag{V.3}$$

The central problem, then, is the reduction of this direct product of irreducible representations to a direct sum. The coefficients of the irreducible representations in the direct sum have been calculated and tabulated by Birman [20]. We use the point group of the point of highest symmetry because all the groups of other points will be subgroups of that group. The O_h group is the point group for the Γ point in the diamond crystal structure. For a phonon decay channel to be infrared allowed, which is what we need for the anti-symmetric excited vibrational state to decay into it, the direct sum must contain the $\Gamma^{(15-)}$ irreducible representation in the O_h point group. This is the irreducible representation of the dipole moment operator, μ, which is the operator that describes IR activity. The two- and three-phonon decay channels and their activation were also calculated by Birman [21], but an example is included to illustrate the principle. The critical symmetry points, the phonons at those points and their symmetry irreducible representations are included in Table II. We know from

Critical point	Phonon	Symmetry	Critical point	Phonon	Symmetry
Γ	$O(\Gamma)$	$\Gamma^{(25+)}$	L	$TO(L)$	$L^{(3-)}$
X	$TO(X)$	$X^{(4)}$		$LO(L)$	$L^{(1+)}$
	$L(X)$	$X^{(1)}$		$LA(L)$	$L^{(2-)}$
	$TA(X)$	$X^{(3)}$		$TA(L)$	$L^{(3+)}$

TABLE II: High symmetry points, phonons, and symmetry species in diamond

the three-phonon density of states (see Section V A) that for the Si decay channel we need 2TO phonons and 1TA phonon. For the example combination mentioned above, TO(L) + TA(L) + TO(X), the calculation of the direct sum is as follows:

$$TO(L) + TA(L) + TO(X) \rightarrow L^{(3-)} \otimes L^{(3+)} \otimes X^{(4)} \tag{V.4}$$

$$= \left(\Gamma^{(2-)} \oplus \Gamma^{(12-)} \oplus 2(\Gamma^{(25-)} \oplus X^{(1)} \oplus X^{(1)} \oplus X^{(2)} \oplus X^{(3)} \oplus X^{(4)})\right) \otimes X^{(4)} \tag{V.5}$$

$$= 12(X^{(1)} \oplus X^{(2)} \oplus X^{(3)}) \oplus 11X^{(4)} \oplus 2(\Gamma^{(1+)} \oplus \Gamma^{(1-)} \oplus \Gamma^{(2+)} \oplus \Gamma^{(2-)})$$
$$\oplus 4(\Gamma^{(12+)} \oplus \Gamma^{(12-)}) \oplus 6(\Gamma^{(15+)} \oplus \Gamma^{(15-)} \oplus \Gamma^{(25+)} \oplus \Gamma^{(25-)}) \qquad \text{(V.6)}$$

So this three-phonon mode contains the required $\Gamma^{(15-)}$ irreducible representation, with a multiplicity/activity of six. Tables III and IV list the infrared allowed three-phonon combinations, 2TO + 1TA phonons for Si and 3TO phonons for Ge, and their multiplicities.

Three-phonon combination	Multiplicity	Frequency (cm^{-1})
TO(X)+TA(X)+O(Γ)	3	1129
TO(L)+TA(L)+O(Γ)	6	1122
TO(L)+TA(L)+TO(X)	6	1071
2TO(X)+TA(X)	2	1078
2TO(L)+TA(X)	3	1134
total	20	

TABLE III: Infrared active three-phonon combinations in silicon

Three-phonon combination	Multiplicity	Frequency (cm^{-1})
2TO(X)+O(Γ)	1	856
2TO(L)+O(X)	3	857
total	4	

TABLE IV: Infrared active three-phonon combinations in germanium

As is clear from the tables, the accepting phonon combination in Si has much higher IR activity than that in Ge, a multiplicity of 20 versus 4. The frequency of the asymmetric stretch mode in Ge falls on a Raman active band (see Appendix C, and therefore has many fewer infrared active modes for the LVM to couple to. This disparity in density of accepting modes between silicon and germanium is a good explanation for the factor of ten difference in their lifetimes.

VI. CONCLUSIONS

We have measured the vibrational lifetimes of the asymmetric stretch mode of oxygen isotopes in silicon and germanium. The measured lifetimes corroborate results from frequency domain measurements. In silicon, the ^{17}O mode falls on the peak of the phonon density of states, which explains the much shorter lifetime (T_1=4.5ps) for this mode when compared to ^{16}O and ^{18}O modes ($T_1 \approx$10ps), which fall to the sides of the peak and have a lower density of states to couple to. The lifetime of ^{16}O in germanium is much longer, which can be explained by the difference in infrared activity between the 2TO + TA phonon decay channels of the silicon modes and the 3TO channels in germanium.

APPENDIX A: FIRST ORDER PHONON DISPERSION RELATIONS

In the simplest case, a crystal may be approximated by an elastic continuum, neglecting the specific atomic structure of the crystal and treating it as a homogeneous continuum. This approximation is only valid if the wavelength λ of elastic waves is much greater than the size of the unit cell in the crystal. Without detailing the derivation, we find that the equation of motion can be calculated from the strain on each end of an element Δx of the band, displaced from equilibrium by an amount u and the density of the elastic material. This strain ($e(x)$) is equal to the force (mass times acceleration):

$$c'(e(x+\Delta x) - e(x)) = \frac{c'\partial^2 u}{\partial x^2}\Delta x = F = \rho \Delta x \frac{\partial^2 u}{\partial t^2}, \tag{A.1}$$

where c' is the stiffness of the continuum, and ρ is the linear density of the material. This is of the form of the wave equation,

$$\frac{\partial^2 u}{\partial x^2} = \frac{1}{v_0}\frac{\partial^2 u}{\partial t^2}, \tag{A.2}$$

where $v_0 = \sqrt{c'/\rho}$ is the velocity of sound in the medium. Solutions are in the form of a travelling wave, and the *dispersion relation*, the relation between frequency ν and the wavevector $\vec{k}$ of the elastic wave, derived from this is linear,

$$\omega = v_0 k. \tag{A.3}$$

In this approximation, the material is said to be dispersion free, since the group velocity of the travelling wave equals the phase velocity.

To go to shorter wavelengths, where $\lambda \approx a$, the crystal may be considered an array of harmonic oscillators of mass m, the bonds between them indicated by a spring with a force constant g which indicates the bond strength. Using only nearest neighbors in the calculation, the equation of motion is the standard $F = kx$ (Hooke's Law spring equation):

$$\frac{\partial^2 u}{\partial x^2} = \frac{1}{m}F = \frac{1}{m}\sum_l g(u_{l+1} - u_l), \tag{A.4}$$

where u_l and u_{l+1} represent the displacement of neighboring atoms. The solutions are again travelling waves, $u_l = u_0 e^i ka - \omega t$. Substituting this into Eq. A.4 and solving

for ω gives the following dispersion relation:

$$\omega = \sqrt{\frac{4g}{m}} \left| \sin \frac{1}{2} ka \right|. \tag{A.5}$$

This equation is periodic in k over a range of $\frac{2\pi}{a}$. To allow momenta in both directions, the range $-\frac{\pi}{a} < k \leq \frac{\pi}{a}$, which is known as the first Brillouin zone (see Section II A), is taken as the cut-off of the possible values of k.

To describe lattices with two or more types of atoms in the unit cell, which is the last approximation we will discuss, consider an array of harmonic oscillators with atoms of different masses, m_1 and m_2, in alternating positions. The equations of motion can be similarly calculated and the resulting dispersion relation is

$$4\omega^2 = g\left(\frac{1}{m_1} + \frac{1}{m_2}\right) \pm g\left[\left(\frac{1}{m_1} + \frac{1}{m_2}\right)^2 - \frac{4\sin^2 ka}{m_1 m_2}\right]^{\frac{1}{2}} \tag{A.6}$$

Clearly, this relation has two solutions. They are called the *acoustic* branch, which corresponds to the different atoms moving in the same direction, as would be expected with the propagation of a sound wave, and the *optical* branch, which is associated with the different atom types moving in opposite directions. The term "optical" arises because this contra-motion can cause electric polarization which can be excited by light incident on the crystal. The optical branches are higher in energy and are less dispersive than the acoustic branches [2, 22].

Additional features of the dispersion relation emerge from consideration and inclusion of the effects of a finite crystal, which has boundaries, generalization to three dimensions, and longitudinal versus transverse wave motion. The optical and acoustic branches split into, in order of decreasing frequency/energy, transverse optical (TO), longitudinal optical (LO), longitudinal acoustic (LA), and transverse acoustic (TA) branches.

APPENDIX B: GROUP THEORY AND SOLID STATE PHYSICS

Group theory is the study of mathematical groups and their properties. It is a powerful formal analytical tool, and can be very useful in analyzing systems that have certain symmetries.

A group can be a set of operators that satisfy the following four properties:

1. The product of two operators that are members of the group must also be a member of the group.

2. Multiplication is associative.

3. There must be an identity operator that commutes with all the other operators and leaves them unchanged.

4. Each operator in the group must have an inverse that is also a member of the group.

In chemistry and solid-state physics, the operators correspond to physical symmetries of the system operators. When applied to a molecule, a symmetry operator is a rotation or reflection that moves the molecule to a new orientation that is equivalent to its original one. There are five types of symmetry operators:

E: The identity operator does nothing to the molecule, it is necessary to satisfy the third property of a mathematical group.

σ: Reflection through a mirror plane. There are several types of mirror planes, depending on their orientation to any rotational symmetry axes.

C_n: Rotation about an axis. The subscript n indicates the fraction of a complete rotation (2π) that is to be performed; the angle is $\frac{2\pi}{n}$.

S_n: Improper rotation corresponds to a C_n rotation followed by a σ reflection through a mirror plane perpendicular to the C_n axis.

i: Inversion involves passing each atom through the (inversion) center of the molecule and placing it on the opposite side. It is equivalent to S_2, but is always given the symbol i. [23]

These symmetry operators can be so assembled as to satisfy all the properties of a mathematical group. These are called *point groups* because there is at least one point in space that is invariant under all the operations in the group. Molecules are then classified as belonging to a certain point group based on their symmetry. The undistorted molecule remains unchanged under all of the operations in the group.

This classification of molecules into point groups is done using the equilibrium configuration, but in the study of molecular vibrations, the distorted configuration is more relevant. The effect of a symmetry operator on a distorted molecule can be described by a linear transformation of coordinates. There are transformations that correspond to each of the symmetry operations, and they also form a group. Two groups (here, symmetry operators and linear transformations) that are related in this way are called *isomorphic*. The transformations can be written in an infinite number of coordinate systems, and in an arbitrary coordinate system, a new coordinate may depend on more than one of the previous coordinates. However, by changing coordinates, it is possible to simplify any one transformation to a *diagonal* form, where each coordinate is transformed into some multiple of itself. It is not generally possible to find a coordinate change that will reduce all the transformations corresponding to the group operators simultaneously to a diagonal form. However, there exist coordinate systems in which the set of transformations in the group are *irreducible*, i.e., the transformations are block diagonal, and cannot be diagonalized further by applying symmetry transformations [24].

Any two representations of a group are either *equivalent,* in which case they can be transformed into one another via symmetry operations using the group elements, or they are *inequivalent,* in which they cannot be transformed into one another. Each point group has a finite number of unique, inequivalent irreducible representations; any representation of the group can be transformed into one of these.

The completely reduced transformations form a representation of the group, and are called the *irreducible representations* of the group. Tables V and VI below are *character tables* for two of the relevant point groups for diamond crystal structures. The top row is the symmetry operators and the first column is the irreducible representations. The numbers indicate the character of the relation between the two. The A_n are non-degenerate, a 1 indicating symmetry under that operator and a -1 indicating anti-symmetry. The E_n are doubly-degenerate and the F_n are triply-degenerate. Their characters are the trace of the matrix representation relating the two or three coordinates to the symmetry operator. These characters are useful in calculating symmetry selection rules for vibrational interactions.

For any physical system such as a molecule, one can construct a character table de-

representations			E	$2C_3$	$3C_2$	i	$2S_6$	$3\sigma_d$
L_1	$L^{(1-)}$	A_{1g}	1	1	1	1	1	1
L_2	$L^{(2-)}$	A_{2g}	1	1	-1	1	1	-1
L_3	$L^{(3-)}$	E_g	2	-1	0	2	-1	0
$L_{1'}$	$L^{(1+)}$	A_{1u}	1	1	1	-1	-1	-1
$L_{2'}$	$L^{(2+)}$	A_{2u}	1	1	-1	-1	-1	1
$L_{3'}$	$L^{(3+)}$	E_u	2	-1	0	-2	1	0

TABLE V: D_{3d} point group symmetry operators and irreducible representations

representations			E	$8C_3$	$3C_2$	$6C_4$	$6C_2'$	i	$8S_6$	$3\sigma_h$	$6S_4$	$6\sigma_d$
Γ_1	$\Gamma^{(1+)}$	A_{1g}	1	1	1	1	1	1	1	1	1	1
Γ_2	$\Gamma^{(2+)}$	A_{2g}	1	1	1	-1	-1	1	1	1	-1	-1
Γ_{12}	$\Gamma^{(12+)}$	E_g	2	-1	2	0	0	2	-1	2	0	0
$\Gamma_{15'}$	$\Gamma^{(15+)}$	F_{2g}	3	0	-1	-1	1	3	0	-1	-1	1
$\Gamma_{25'}$	$\Gamma^{(25+)}$	F_{1g}	3	0	-1	1	-1	3	0	-1	1	-1
$\Gamma_{1'}$	$\Gamma^{(1-)}$	A_{1u}	1	1	1	1	1	-1	-1	-1	-1	-1
$\Gamma_{2'}$	$\Gamma^{(2-)}$	A_{2u}	1	1	1	-1	-1	-1	-1	-1	1	1
$\Gamma_{12'}$	$\Gamma^{(12-)}$	E_u	2	-1	2	0	0	-2	1	-2	0	0
Γ_{15}	$\Gamma^{(15-)}$	F_{2u}	3	0	-1	-1	1	-3	0	1	1	-1
Γ_{25}	$\Gamma^{(25-)}$	F_{1u}	3	0	-1	1	-1	-3	0	1	-1	1

TABLE VI: O_h point group symmetry operators and irreducible representations

scribing the group symmetry operations on the molecular coordinates. These tables, combined with the tables for the irreducible representations, can be used to determine how many instances of particular irreducible representation are present for that specific system. This in turn helps to determine selection rules for specific quantum transitions.

APPENDIX C: SYMMETRY SELECTION RULES

There are two types of spectroscopic activation for a vibrational mode in a crystal: Raman and infrared (IR). Infrared activation is probed by measuring the IR absorption of molecule or crystal sample. Light of many different frequencies is passed through the sample and the intensity of the transmitted light is measured at each frequency. The FTIR spectrometer discussed in Section III A is a good example. A vibrational mode will be IR active if the vibration changes the electric dipole moment of the molecule or quasi-molecule. The dipole moment operator, $\vec{\mu} = q\vec{r}$, is said to describe the transition for IR spectroscopy.

Raman spectroscopy does not measure transmitted light, but rather light scattered from the sample. Most of the scattered light has the same frequency ν_0 as the incident light, but a small fraction (about 1/1000) does not have this frequency. Instead, it has frequencies ν_i such that the energy difference $\Delta E = h|\nu_0 - \nu_i|$ corresponds to energies that are absorbed by the sample. The incident frequency ν_0 is usually in the visible, but the difference $|\nu_0 - \nu_i|$ is in the infrared, since it corresponds to vibrational frequencies. The light with frequency $\nu_i < \nu_0$ is called *Stokes* radiation, and is much more common than *anti-Stokes* radiation, which is light with frequency $\nu_i > \nu_0$. A mode is Raman active if the vibration changes the polarizability tensor, also called the Raman scattering tensor or just the Raman tensor. The Raman tensor is denoted $\hat{\alpha}$.

The activity of a mode is described by a transition matrix element that indicates the probability of the transition from the ground state to the excited state corresponding to the mode in question. The transition probability amplitude is

$$M_{\nu\nu'} = \langle \psi(\nu') \mid \hat{\wp} \mid \psi(\nu) \rangle = \int_{-\infty}^{\infty} \psi^*(\nu')\, \hat{\wp}\, \psi(\nu) d\vec{r}. \tag{C.1}$$

The transition $\nu \rightarrow \nu'$ is active if this matrix element is non-zero, with $\hat{\wp}$ is $\hat{\mu}$ for IR activation, and $\hat{\alpha}$ for Raman activation. Basically, for the transition probability will only be non-zero if the integrand $\psi^*(\nu')\, \hat{\wp}\, \psi(\nu)$ is symmetric. An integral from $-\infty$ to ∞ over an anti-symmetric function will always be zero.

The electric dipole operator is always anti-symmetric, since it is just a constant times $\vec{r}$, which is anti-symmetric. In Si, the Raman tensor $\hat{\alpha}$ is symmetric. The

ground state, ψ_0 is unchanged under any of the symmetry operators, and is therefore always totally symmetric. The excited state corresponding to the anti-symmetric stretch mode is anti-symmetric. The integrand is then one symmetric function and two anti-symmetric functions, so it is overall symmetric, the transition probability is non-zero and the mode is IR active.

For example, to verify that the anti-symmetric stretch mode is IR active, the matrix element is

$$M = \langle \psi_0 | \vec{\mu} | \psi_1 \rangle = A_{1g} \otimes (E_u \oplus A_{2u}) \otimes A_{2u} = (E_u \oplus A_{2u}) \otimes A_{2u}, \tag{C.2}$$

where A_{1g} is the totally symmetric irreducible representation in the D_{3d} group, $(E_u \oplus A_{2u})$ is the representation of the dipole operator, and A_{2u} is the representation of the asymmetric stretch mode. The representation A_{1g} is the identity for multiplication. Using the character table in Table V, the direct product is the following

$$\begin{aligned} & (\langle 1,1,-1,-1,-1,1\rangle \oplus \langle 2,-1,0,-2,1,0\rangle) \otimes \langle 1,1,-1,-1,-1,1\rangle \\ = \; & \langle 3,0,-1,-3,0,1\rangle \otimes \langle 1,1,-1,-1,-1,1\rangle \\ = \; & \langle 3,0,1,3,0,1\rangle \\ = \; & \langle 2,-1,0,2,-1,0\rangle \oplus \langle 1,1,1,1,1,1\rangle \end{aligned} \tag{C.3}$$

One can see by inspection that this is the direct sum $E_g \oplus A_{1g}$, which contains the totally symmetric representation A_{1g} and therefore the asymmetric stretch mode is IR active.

ACKNOWLEDGMENTS

The author acknowledges Dr. Gunter Lüpke and Baozhou Sun for assistance, advice, and expertise on every aspect of this thesis. Our excellent samples were provided by collaborators R. C. Newman at the Imperial College, London, and B. Pajot at Universités Pierre et Marie Curie et Denis Diderot, Paris, who also contributed through productive discussions. We are grateful for the assistance of the technical staff at Jefferson Lab's FEL Facility. This work was supported by the NSF through grant DMR-02-42316.

[1] M. Balkanski and R. F. Wells, *Semiconductor Physics and Applications* (Oxford University Press, 2000).

[2] H. P. Myers, *Introductory Solid State Physics* (Taylor & Francis, 1990).

[3] P. Giannozzi, S. de Gironcoli, P. Pavone, and S. Baroni, Phys. Rev. B **43** (1991).

[4] S. Wei, C. Li, and M. Y. Chou, Phys. Rev. B **50**, 14587 (1994).

[5] S. Wei and M. Y. Chou, Phys. Rev. B **50** (1994).

[6] M. D. McCluskey, Appl. Phys. Rev. **87**, 3593 (2000).

[7] G. Lüpke, N. H. Tolk, and L. C. Feldman, Appl. Phys. Rev **93**, 2317 (2003).

[8] F. Shimura, ed., *Oxygen in Silicon: Semiconductors and Semimetals*, vol. 42 of *Semiconductors and Semimetals* (Academic Press, 1994).

[9] W. Kaiser, P. H. Keck, and C. F. Lange, Phys. Rev. **101** (1956).

[10] E. Artacho, F. Ynduráin, B. Pajot, R. Ramirez, C. P. Herrero, L. I. Khirunenko, K. M. Itoh, and E. E. Haller, Phys. Rev. B **56**, 3820 (1997).

[11] H. J. Hrostowski and R. H. Kaiser, Phys. Rev. **107** (1957).

[12] L. Hsu, M. D. McCluskey, and J. L. Lindström, Phys. Rev. Lett. **90**, 95505 (2003).

[13] A. Nitzan and J. Jortner, Mole. Phys. **25** (1973).

[14] A. Nitzan, S. Mukamel, and J. Jortner, J. Chem. Phys. **60** (1974).

[15] S. P. Davis, M. C. Abrams, and J. W. Brault, *Fourier Transform Spectrometry* (Academic Press, 2001).

[16] J. Y. Zhang, J. Y. Huang, and Y. R. Shen, *Optical Parametric Generation and Amplification*, vol. 19 of *Laser Science and Technology* (Harwood Academic Publishers, 1995).

[17] C. L. Tang and L. K. Cheng, *Fundamentals of Optical Parametric Processes and Oscillators*, vol. 20 of *Laser Science and Technology* (Harwood Academic Publishers, 1995).

[18] B. Pajot, E. Artacho, C. A. J. Ammerlaan, and J.-M. Spaeth, J. Phys.: Condens. Matter **7** (1995).

[19] B. Pajot, P. Clauws, J. L. Lindström, and E. Artacho, Phys. Rev. B **62**, 10165 (2000).

[20] J. L. Birman, Phys. Rev. **127**, 1093 (1962).

[21] J. L. Birman, Phys. Rev. **131**, 1489 (1963).

[22] P. M. A. Sherwood, *Vibrational Spectroscopy of Solids* (Cambridge University Press, 1972).

[23] D. C. Harris and M. D. Bertolucci, *Symmetry and spectroscopy: An introduction to vibrational and electronic spectroscopy* (Oxford University Press, 1978).

[24] E. B. Wilson, J. C. Decius, and P. C. Cross, *Molecular Vibrations* (McGraw-Hill Book Company, Inc., 1955).